




Effect of functional on structural, elastic stability, optoelectronic and thermoelectric characteristics of semiconducting MgX_2Se_4 ($\text{X} = \text{Lu}, \text{Y}$) spinels

K BOUFERRACHE¹, M A GHEBOULI^{2,3}, Y SLIMANI⁴, B GHEBOULI⁵, M FATMI^{2,*} , T CHIH², MOHAMED A HABILA⁶, NOUF H ALOTAIBI⁶ and MIKA SILLANPAA^{7,8}

¹Department of Physics, Faculty of Sciences, University of Mohamed Boudiaf, 28000 M'sila, Algeria

²Research Unit on Emerging Materials (RUEM), University Ferhat Abbas of Setif 1, 19000 Setif, Algeria

³Department of Chemistry, Faculty of Sciences, University of Mohamed Boudiaf, 28000 Msila, Algeria

⁴Laboratory of Intelligent System (LSI), Faculty of Technology, University Ferhat Abbas of Setif 1, 19000 Setif, Algeria

⁵Laboratory for the Study of Surfaces and Interfaces of Solid Materials (LESIMS), University Ferhat Abbas of Setif 1, 19000 Setif, Algeria

⁶Department of Chemistry, College of Science, King Saud University, PO Box 2455, 11451 Riyadh, Saudi Arabia

⁷Department of Biological and Chemical Engineering, Aarhus University, Norrebrogade 44, 8000 Aarhus C, Denmark

⁸School of Technology, Woxsen University, 502345 Telangana, India

*Author for correspondence (fatmimessaoud@yahoo.fr)

MS received 27 September 2023; accepted 30 January 2024

Abstract. Effect of functional on structural, elastic, optoelectronic and thermoelectric characteristics of semiconducting MgX_2Se_4 ($\text{X} = \text{Lu}, \text{Y}$) spinels has been realized by WIEN2k code. The lattice constant of MgY_2Se_4 is slightly greater than that of MgLu_2Se_4 , and these quantities are slightly deviated from the experimental values, where the error does not exceed 1.3%. The cohesive energy proves that both spinels are chemically stable in the normal case, and this stability is more pronounced in MgLu_2Y_4 . The large ionic radius of Lu compared to Y explains the high bulk modulus of MgY_2Se_4 as well as its hardness. The spinels under study have $\Gamma \rightarrow \Gamma$ direct band gap located between 1.178 and 1.4 eV for all the functionals, proving their semiconductor nature. Se-s, Y-d, Lu-d states in MgY_2Se_4 and MgLu_2Se_4 dominate the upper valence band, while the first conduction band located between Fermi level and 1.5 eV is empty. There is a strong coupling between Se-p–Lu-p sites for MgLu_2Se_4 and Se-p–Y-p states in MgY_2Se_4 , which reflects their hybridization. The high absorption in the ultraviolet range, the band gap between 1 and 2.4 eV and the refractive index in the range of 2.29–2.61 favour these spinels as absorbers in solar cells. Peaks of all the optical quantities studied relating to the mBJ–GGA functional are shifted to the right compared with GGA and GGA+SO approximations. The thermoelectric parameters were investigated as a function of photon energy and temperature using GGA+SO functional.

Keywords. MgY_2Se_4 ; MgLu_2Se_4 ; CASTEP; DFT; elastic properties; electronic properties.

1. Introduction

Spinel materials crystallize in a cubic structure, have the stoichiometric formula AB_2C_4 and show a particular interest because of their applications in energy storage, optical and photonic devices. The C anions are arranged in a closed cubic lattice, while the A and B cations are arranged in the octahedral and tetrahedral positions. Magnesium-based spinels are of more interest for their use as metallic cathodes in batteries [1], and have appropriate electrochemical and thermoelectric properties [2,3]. Wang *et al* [4] investigated the effect of cation and anion variances on the elastic and electronic properties of a variety of spinels. The novelty of this study lies in the search of new spinels, such as MgLu_2Y_4 and MgLu_2Se_4 having adequate electronic, optical and thermoelectric parameters.

Mg-based spinels are promising materials for batteries, in thermoelectric and optoelectronic applications and motivate researchers to find new suitable materials. Adequate optical and electrical properties of such spinels allow their use in lasers, optoelectronic devices and energy storage, such as super capacitors and solar cells [5–8]. Mechanical, optoelectronic and thermoelectric properties of CdLu_2X_4 ($\text{X} = \text{S}, \text{Se}$) were carried out by Fasih Zareef *et al* [9] using WIEN2k. Mustafa *et al* [10] studied optoelectronic and transport properties of MgLu_2Se_4 . Pham *et al* [11] investigated the structural, elastic, electronic and optical properties of MgSc_2X_4 ($\text{X} = \text{S}, \text{Se}$). Among a variety of spinel materials based on yttrium and lutetium, we explore in this study MgX_2Se_4 ($\text{X} = \text{Lu}, \text{Y}$) compounds using density functional theory (DFT) based on WIEN2k code. We report a detailed

Table 1. The values of $R_{MT} \cdot K_{max}$, R_{MT} of each constituent and k-point for MgX_2Se_4 ($X = Lu, Y$) using GGA and GGA+mBJ and GGA+SO.

Spinel	Approach	$R_{MT} \cdot K_{max}$	R_{MT} (Mg)	R_{MT} (X)	R_{MT} (Se)	k-point
$MgLu_2Se_4$	GGA	8.5	2.14	2.50	2.37	1000
MgY_2Se_4	GGA	8.5	2.10	2.50	2.32	1000

Table 2. The values of lattice constant, bulk modulus and its pressure derivative, volume, and minimum energy of MgX_2Se_4 ($X = Lu, Y$) spinels.

Compound	Parameter	GGA	
		Normal	Inverse
$MgLu_2Se_4$ 227_ $Fd\bar{3}m$	a (Å)	11.536 11.43 exp. [18] 11.539 [19]	11.5756 11.43 exp. [18]
	$\frac{\Delta a}{a}$	0.009	0.0127
	B (GPa)	58.813 58.874 [19]	57.266
	B'	4.078 4.062 [19]	4.1186
	V_0 (Å) ³	2590.5590	2616.7649
	E_{min} (Ry)	−156336.037374	−156335.884101
	a (Å)	11.6845 11.57 exp. [18]	11.7313 11.57exp. [18]
MgY_2Se_4 227_ $Fd\bar{3}m$	$\frac{\Delta a}{a}$	0.0098	0.0139
	B (GPa)	56.6178	54.6073
	B'	4.1029	4.0233
	V_0 (Å) ³	2691.3485	2723.8104
	E_{min} (Ry)	−66772.627836	−66772.496660

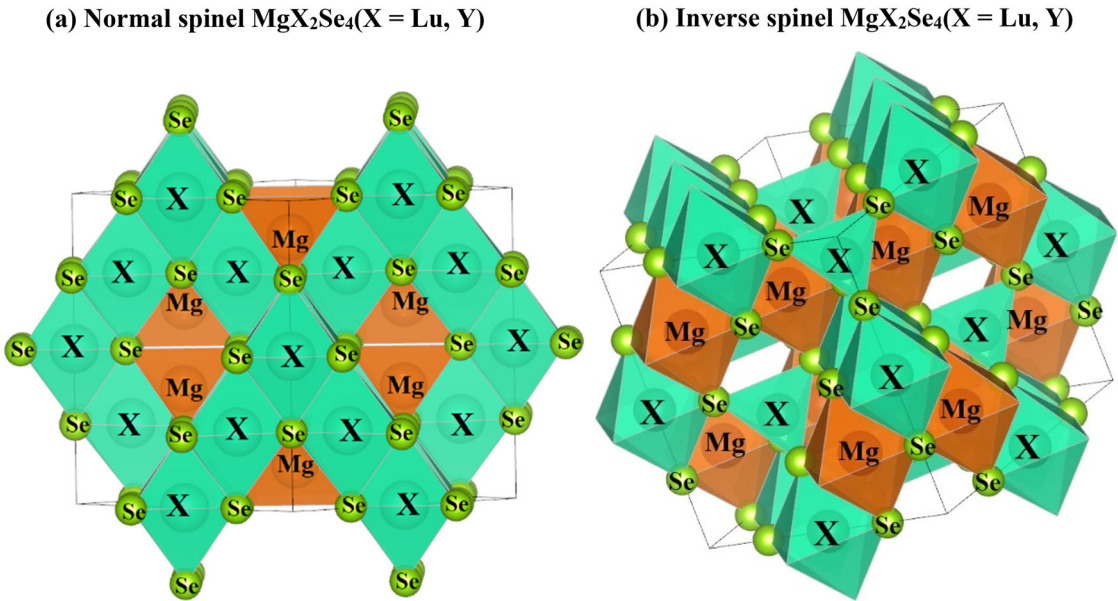


Figure 1. Spinel structure in the (a) normal and (b) inverse states for MgX_2Se_4 ($X = Lu, Y$) spinel.

Table 3. Elastic constants, C_{ij} (GPa); Cauchy pressure, C_P (GPa); bulk modulus, B (GPa); shear modulus, G (GPa); Young’s modulus, E (GPa); Poisson’s ratio, σ ; and Pugh’s index, B/G for both spinels MgX_2Se_4 ($X = Lu, Y$).

Spinel	C_{11}	C_{12}	C_{44}	C_P	B	G	E	σ	B/G
$MgLu_2Se_4$	81.66	56.72	27.11	29.61	65.03	21.25	57.49	0.35	3.06
	128.63 [19]	23.99 [19]	28.96 [19]	−4.97 [19]	58.87 [19]	36.78 [19]	91.33 [19]	0.24 [19]	1.60 [19]
MgY_2Se_4	78.08	55.47	24.57	30.90	63.00	19.26	52.44	0.36	3.27

investigation of structural, elastic, electronic, optical and thermoelectric properties of these spinels [12–14]. In this paper, all the properties relating to MgY_2Se_4 are investigated for the first time. The study of various properties of these two spinels was carried out using GGA, mBJ–GGA and

GGA+SO. The intense amount of absorption located in the ultraviolet light as well as their band gap in the range of 1.1–2.2 eV validate the candidature of these spinels as absorbers in solar cells and optoelectronic applications. The rather high absorption of MgX_2Se_4 ($X = Lu, Y$) spinels in the

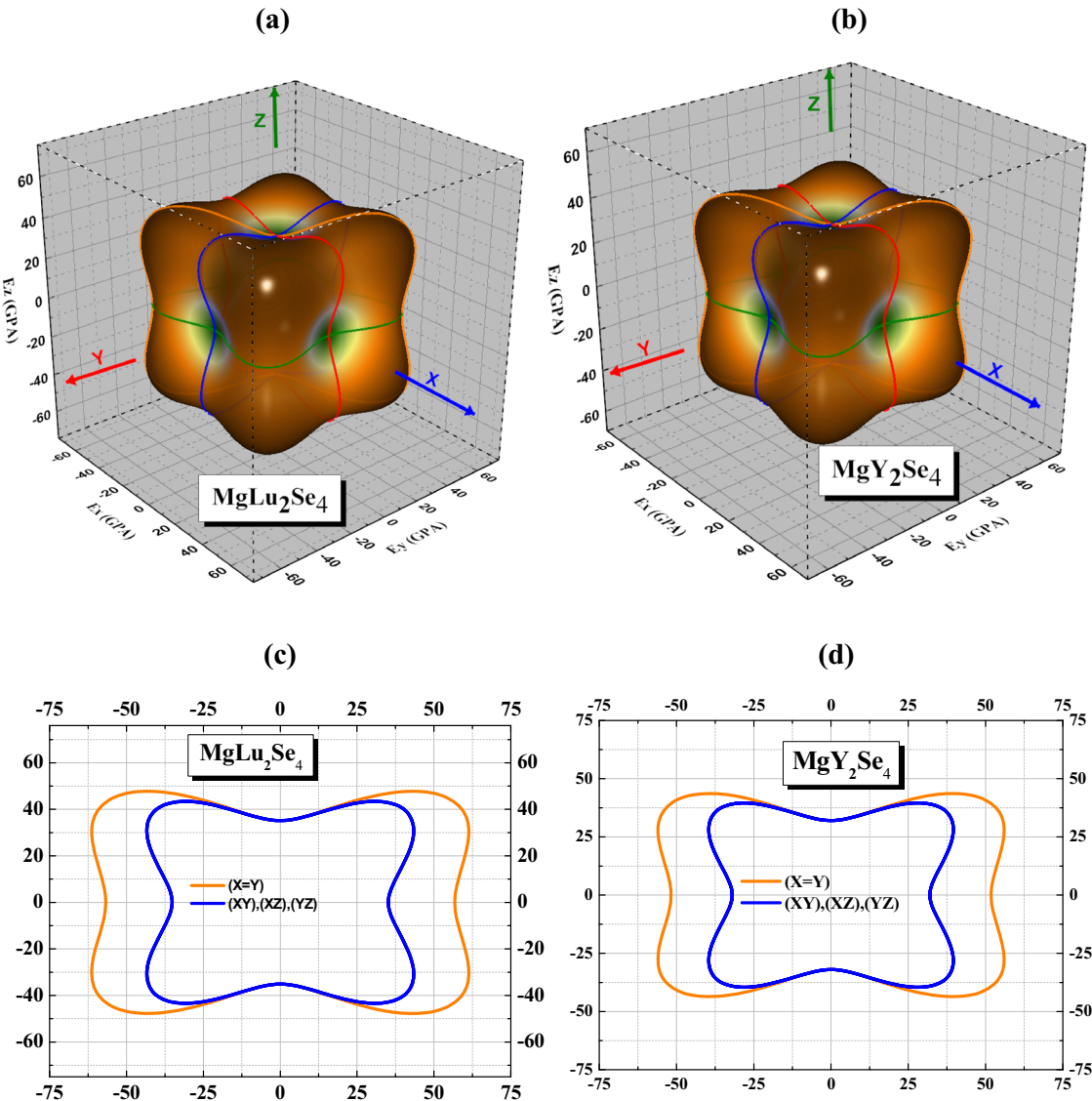


Figure 2. The 3D surfaces of Young’s modulus for (a) $MgLu_2Se_4$ and (b) MgY_2Se_4 and (c and d) their cross-sections in different planes, respectively.

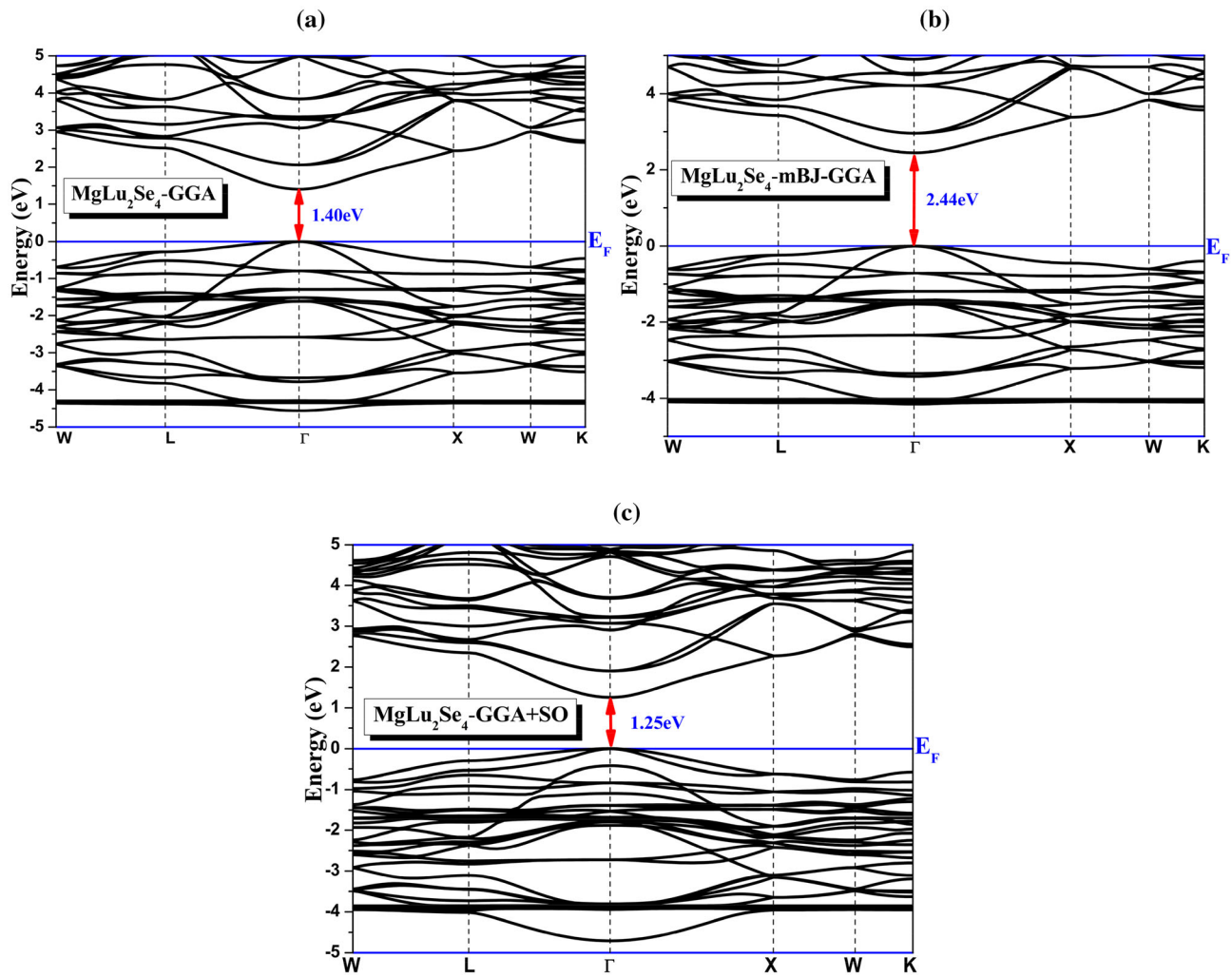


Figure 3. Band structure of MgLu_2Se_4 is calculated by (a) GGA, (b) mBJ-GGA and (c) GGA+SO functionals.

ultraviolet compared to the visible region is a sign of their applications in optoelectronic and thermoelectric fields. The amount of absorption and band gap validate the candidature of MgX_2Se_4 ($X = \text{Lu}, \text{Y}$) spinels as absorber materials for photovoltaic devices. The study of thermoelectric characteristics in this work shows that these two spinels are candidates in thermoelectric application, but MgY_2Se_4 is more advantageous [15].

2. Calculation details

Computations were performed using the WIEN2k code's implementation of the augmented plane-wave plus local orbitals basis functions utilizing the GGA, mBJ-GGA, and GGA+SO approximations [16]. To calculate structural and optical properties, the generalized gradient approximation (GGA) of Perdew, Burke and Ernzerhof is utilized [13]. The modified Becke–Johnson technique is used to calculate the electronic characteristics [17]. The DFT+U approximation is used to handle the electron–electron correlation effect

[15]. Table 1 reports the R_{MT} radius of Lu, Y, Mg and Se. With angular moments up to $l_{\text{max}} = 10$, the spherical harmonic expansion is used to express the charge density and potentials. We employ a plane wave basis with an $R_{\text{MT}} \cdot K_{\text{max}} = 8.5$. For the Brillouin zone integration, a mesh of 1000 k-points guarantees convergence and overall energy minimization. The energy difference between the valence and core states was set to -8 Ry. Convergence was charged at 0.001 e. Due to the dearth of experimental results, our objective is to compare the outcomes of GGA, mBJ-GGA, and GGA+SO functional. In comparison with the functional mBJ, the influence of R_{MT} on electronic parameters is not considerable.

3. Results and discussion

3.1 Structural and elastic stabilities

The spinel structure shows the molecular formula AB_2C_4 , where the C anion forms a compact face-centred cubic

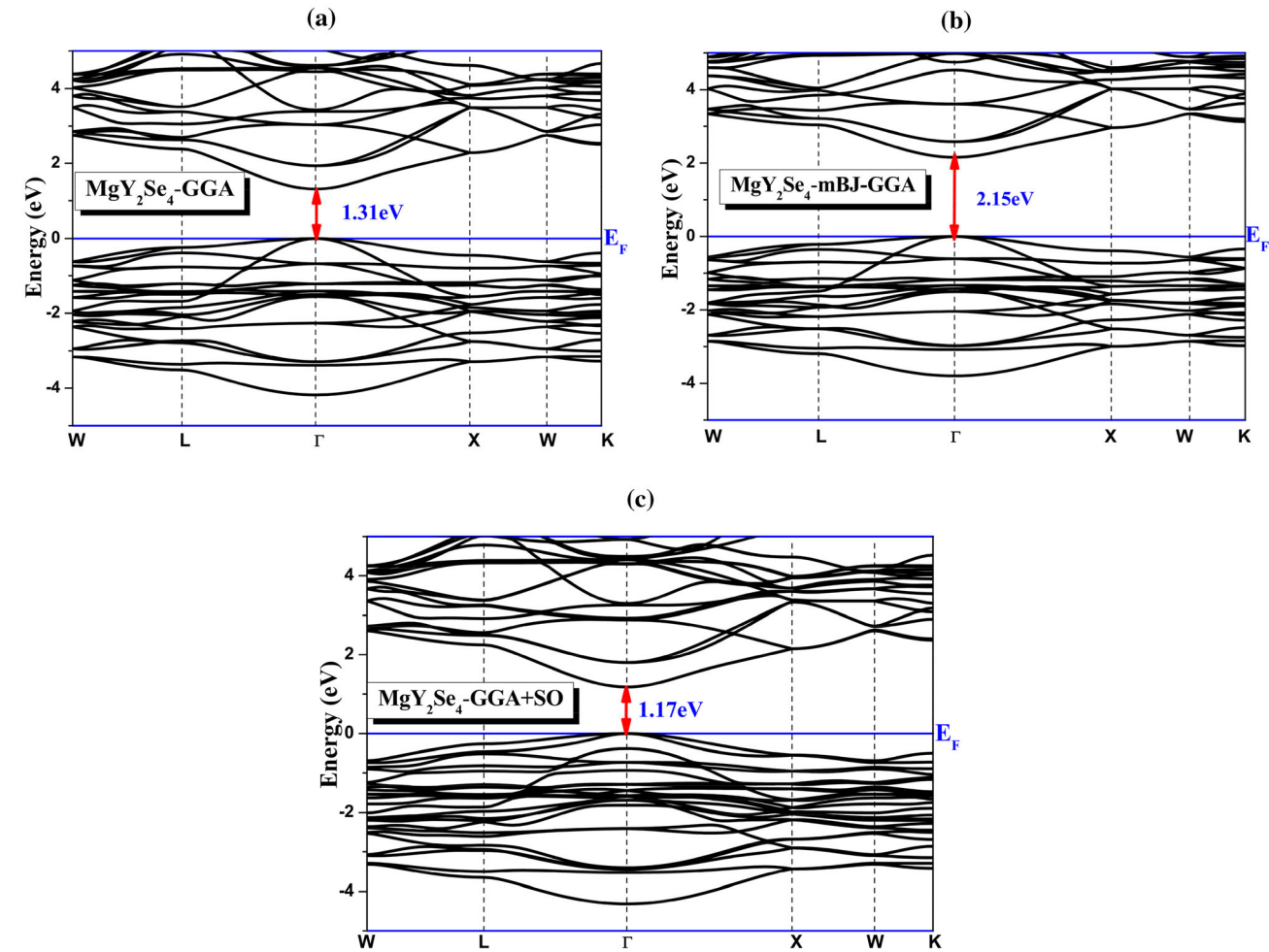


Figure 4. Band structure of MgY_2Se_4 is calculated by (a) GGA, (b) mBJ-GGA and (c) GGA+SO functionals.

Table 4. Values of band gap for MgX_2Se_4 ($X = \text{Lu}, \text{Y}$) spinels using GGA, mBJ-GGA and GGA+SO approximations.

Compound	E_g (eV)		
	GGA	mBJ-GGA	GGA+SO
MgLu_2Se_4	1.40	2.44 2.48 [2]	1.253
$227_F\bar{d}3m$	$\Gamma-\Gamma$	$\Gamma-\Gamma$	$\Gamma-\Gamma$
MgY_2Se_4	1.312	2.153	1.178
$227_F\bar{d}3m$	$\Gamma-\Gamma$	$\Gamma-\Gamma$	$\Gamma-\Gamma$

packing and the A and B cations share octahedral and tetrahedral sites. We discuss in this subsection, the behaviour of structural parameters and cohesive energy for MgX_2Se_4 ($X = \text{Lu}, \text{Y}$) spinels. In table 2, we report the lattice constant, bulk modulus and its pressure derivative, volume and minimum energy of the cubic spinel structure MgX_2Se_4 ($X = \text{Lu}, \text{Y}$) in the normal and inverse cases

using GGA approximation as shown in figure 1. The lattice constants of MgLu_2Se_4 and MgY_2Se_4 in the normal and inverse cases agree well with the experimental values of 11.43 and 11.57 Å, which were reported in the literature [17]. Note that the lattice constant of MgY_2Se_4 is slightly greater than that of MgLu_2Se_4 . It is also noted that the relative error in the calculation of the lattice constant compared to the experimental value is understood to be between 0.9 and 1.3%. The lattice constant and pressure derivative of bulk modulus of MgLu_2Se_4 are in good agreement with their theoretical ones quoted in the literature [18]. The bulk modulus of MgY_2Se_4 is slightly smaller than that of MgLu_2Se_4 , which is explained by the large ionic radius of Lu compared with that of Y. Cohesion energy is a quantity that provides information on the chemical stability of a material. It is expressed by the follow relation:

$$E_{\text{co}} = E_{\text{tot}}^{\text{MgX}_2\text{Se}_4} - \left(E_{\text{Mg}}^{\text{atom}} + 2E_{\text{X}}^{\text{atom}} + 4E_{\text{Se}}^{\text{atom}} \right). \tag{1}$$

Cohesive energy values are listed in table 2. The negative value of total energy is a sign of the chemical stability of these spinels. It is noticed that the two spinels are more

stable in the normal case, and the stability in MgLu_2Se_4 is more pronounced.

Elastic constants, C_{ij} ; Cauchy pressure, C_P ; bulk modulus, B ; Shear modulus, G ; Young modulus, E ; Poisson's ratio, σ and Pugh's index, B/G for both spinels MgX_2Se_4 ($X = \text{Lu}, \text{Y}$) are listed in table 3. The knowledge of the elastic constants informs us about the elastic stability of the structure and the heterogeneous bond between neighbouring atoms. Computed elastic moduli of MgX_2Se_4 ($X = \text{Lu}, \text{Y}$) are positive and satisfying the following generalized conditions to ensure their elastic stability [19]:

$$C_{11} + 2C_{12} > 0, C_{44} > 0, C_{11} - C_{12} > 0, C_{12} < B < C_{11}. \quad (2)$$

The bulk modulus of MgLu_2Se_4 is larger than that of MgY_2Se_4 , and then, MgLu_2Se_4 is more resistant to deformations. Also, shear modulus and Young modulus values of MgLu_2Se_4 are larger than those of MgY_2Se_4 , indicating that MgLu_2Se_4 is more resistant to shear and longitudinal deformations and stiffer than MgY_2Se_4 . Poisson's ratio predicts the nature of bonding and the value of 0.26 separates the ductility to the brittleness. Poisson's ratio values of MgX_2Se_4 ($X = \text{Lu}, \text{Y}$) confirm their metallic bonding class and ductility.

Poisson's ratio in the range of 0.25–0.50 also classifies these two spinels as non-central forces. Shear and Young's moduli describe the stiffness of the bond and the resistance to deformation and fracture. Cauchy pressure specifies the nature of bonds. The positive value of Cauchy pressure $C_P = C_{12} - C_{44}$ indicates that these spinels are ionic bonding in nature. Pugh's index B/G for both spinels MgX_2Se_4 ($X = \text{Lu}, \text{Y}$) are larger than 1.75, which confirms their ductility. The 3D surface of Young's modulus for MgLu_2Se_4 and MgY_2Se_4 and their cross-sections in different planes ($x = y$ red colour, xy , xz and yz blue colour) are visualized in figure 2. A material is considered isotropic when the 3D shape of the Young's modulus is spherical. We noticed that the shape of Young's modulus and cross-sections for various planes are completely deformed, indicating the presence of a strong anisotropy. The cross-sections in the figure of the two spinels show that the anisotropy is less pronounced in the $x = y$ plane. The maximum value of Young's modulus for MgLu_2Se_4 (MgY_2Se_4) is 40, 20 and 10 GPa (60, 30 and 0 GPa) along (x , y and z axes).

3.2 Electronic band structure and density of states

The lattice structure is a determining factor in the electronic structure of a semiconductor. The functional affects the energy gap and its nature, hence, the use of multiple functional to elucidate this effect. Band structures of MgLu_2Se_4 and MgY_2Se_4 calculated by GGA, mBJ-GGA and GGA+SO, are reported in figures 3 and 4. All these functionals reveal a $\Gamma \rightarrow \Gamma$ direct band gap in spinels under study. All band gap values are reported in table 4 and prove that these spinels are semiconductors. GGA+SO is reported

to give the smaller band gap, while mBJ-GGA has the higher band gap for both spinels. The important point that we noted is that the direct band gap is desired in optoelectronic applications. It is reported that the band gap of MgLu_2Se_4 using the GGA-PBE sol is 2 eV [10]. There is no experimental value of the band gap quoted in the literature for the two spinels under study. The lack of an experimental value of a quantity requires the use of several functionals to have the accurate of such quantity. The exploration of electronic behaviour in depth requires the calculation of total and partial densities. TDOS of MgLu_2Se_4 and MgY_2Se_4 calculated by GGA, GGA-mBJ and GGA+SO and PDOS of Mg, Lu and Y atoms computed by GGA are visualized in figures 5 and 6. For both spinels, Se-s, Y-d, Lu-d states dominate in the valence and conduction bands, while the first conduction band located between Fermi level and 1.5 eV is empty.

In the PDOS spectrum, we distinguished a strong coupling Se-p–Lu-p sites and Se-p–Y-p states for MgLu_2Se_4 and MgY_2Se_4 . The TDOS in valence and conduction bands are similar to Se-p and X-d spectrum for MgX_2Se_4 ($X = \text{Lu}, \text{Y}$) in all functional, then, there is a hybridization between Se-p and X-d sites.

3.3 Optical characteristics

The interaction of light with matter is transduced by photon energy transformation, such as absorption, reflectivity and diffusion. (a and b) Real and imaginary parts of dielectric function, (c) refractive index, (d) extinction coefficient, (e) absorption coefficient and (f) reflectivity of MgLu_2Se_4 and MgY_2Se_4 computed by GGA, GGA+SO and mBJ-GGA are reported in figures 7 and 8a–f. The real component explains scattering and reflectivity, while the imaginary part determines the absorption features. The static dielectric function values of MgLu_2Se_4 and MgY_2Se_4 , computed using GGA, GGA+SO and mBJ-GGA, are reported in table 5. The similarity in the effect of photon energy on the real and imaginary components in these two spinels indicates that their optical characteristics are also similar. The extremes situated at 2.5 eV (GGA and GGA+SO) and 3.25 eV (mBJ-GGA) correspond to interband transitions between Mg-p/d and Se-p to the empty conduction band located between Fermi level and 2 eV for both spinels. The static refractive index values of MgLu_2Se_4 and MgY_2Se_4 calculated using GGA, GGA+SO and mBJ-GGA approaches are given in table 5. The maximum of the refraction angle is obtained at photon energies of 3, 3 and 4 eV (2.6, 2.6 and 2.37) using GGA, GGA+SO and mBJ-GGA for MgLu_2Se_4 (MgY_2Se_4). At about energy of 7.5 eV, all the propagating waves are attenuated, because the attenuation coefficient passes through its maximum. The absorption edges at about 1.3 eV (2.2 eV), which corresponds to the band gap located between 1.178 and 1.4 eV

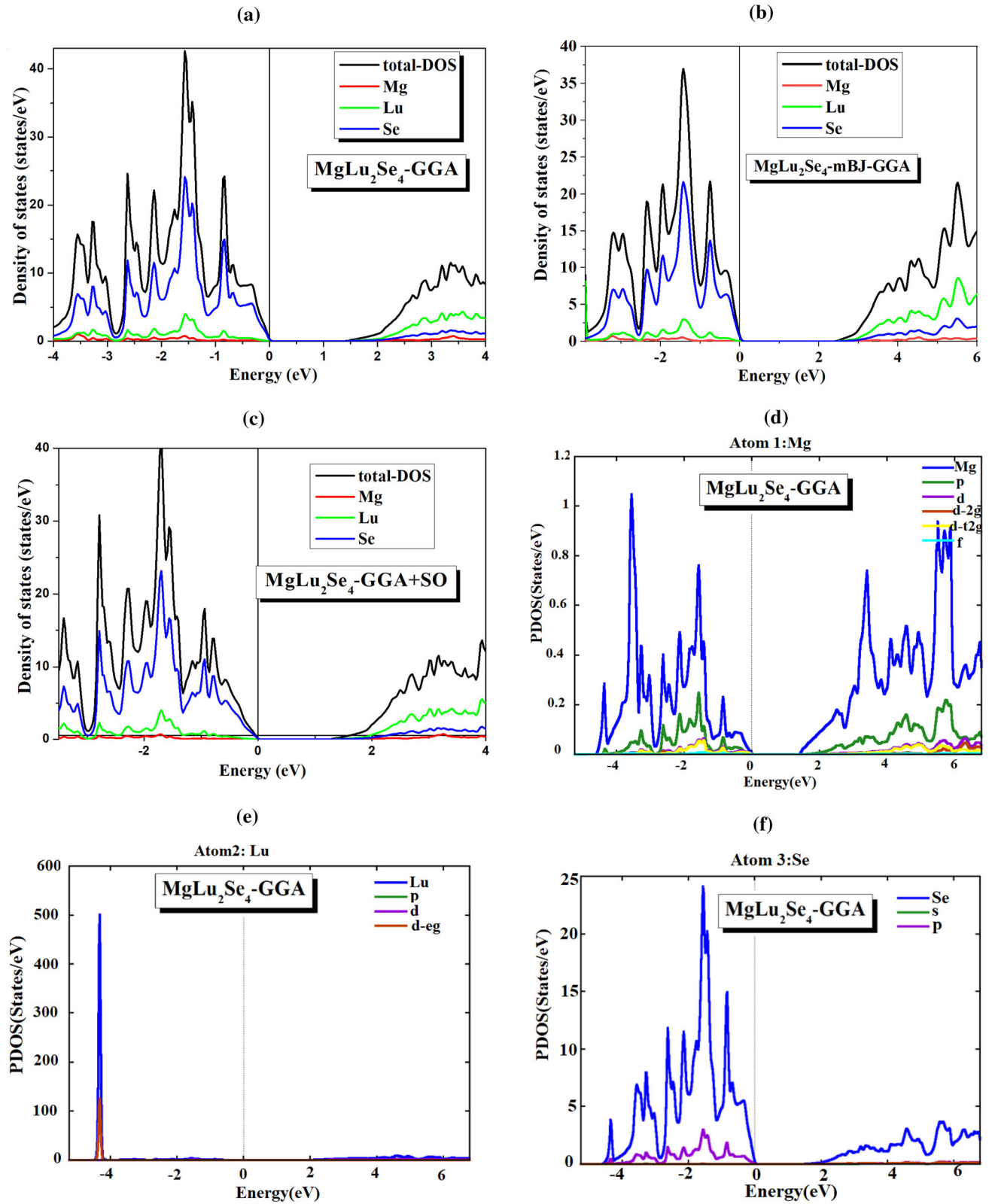


Figure 5. TDOS of MgLu_2Se_4 is calculated by (a) GGA, (b) GGA-mBJ and (c) GGA+SO. PDOS of (d) Mg atom, (e) Lu atom and (f) Se atom is calculated by GGA.

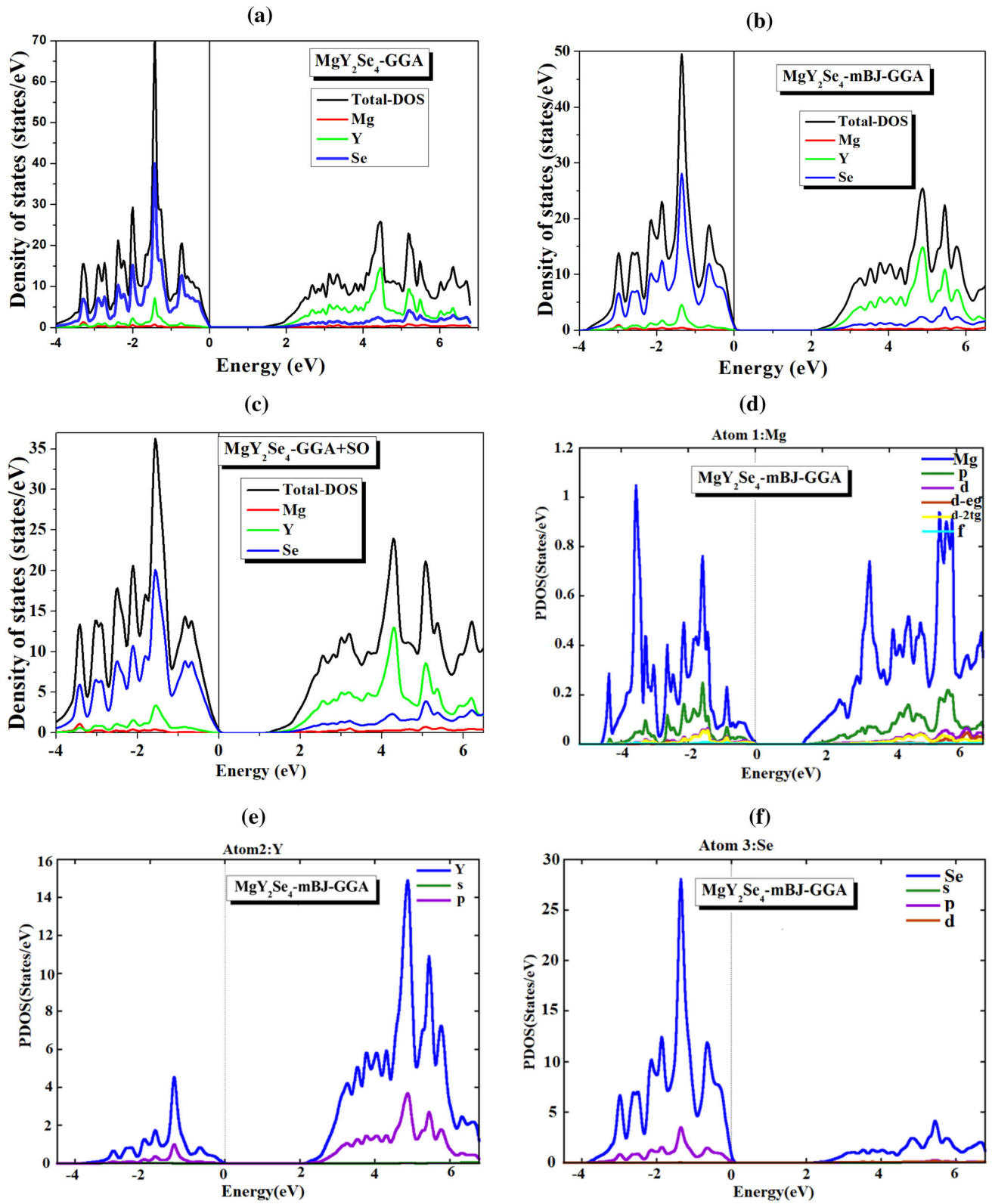


Figure 6. TDOS of MgY_2Se_4 is calculated by (a) GGA, (b) GGA-mBJ, (c) GGA+SO. PDOS of (d) Mg atom, (e) Y atom and (f) Se atom is calculated by GGA-mBJ.

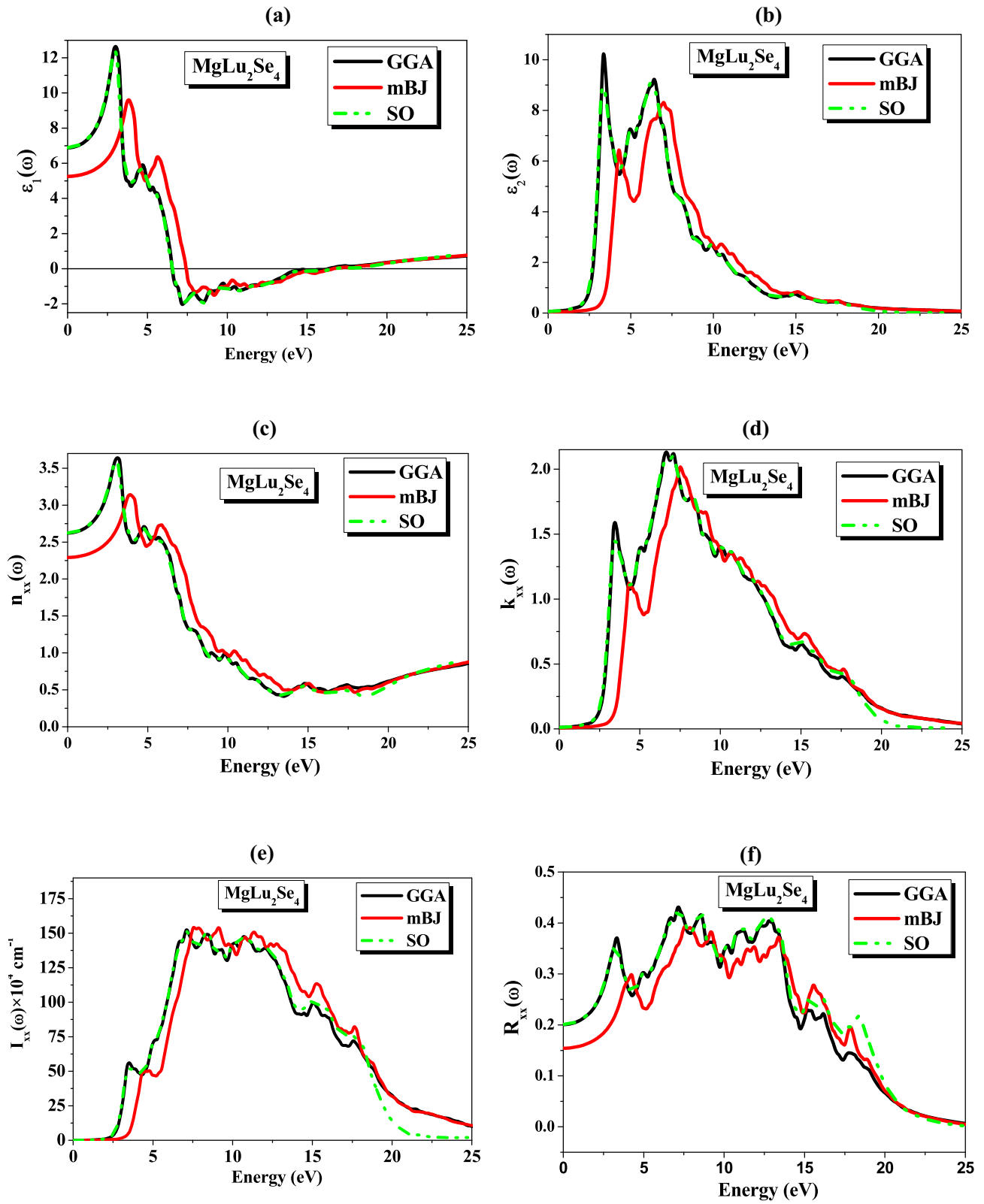


Figure 7. Spectra of (a) real and (b) imaginary dielectric functions, (c) refractive index, (d) extinction coefficient, (e) absorption coefficient and (f) reflectivity of MgLu_2Se_4 calculated by GGA, mBJ–GGA and GGA+SO.

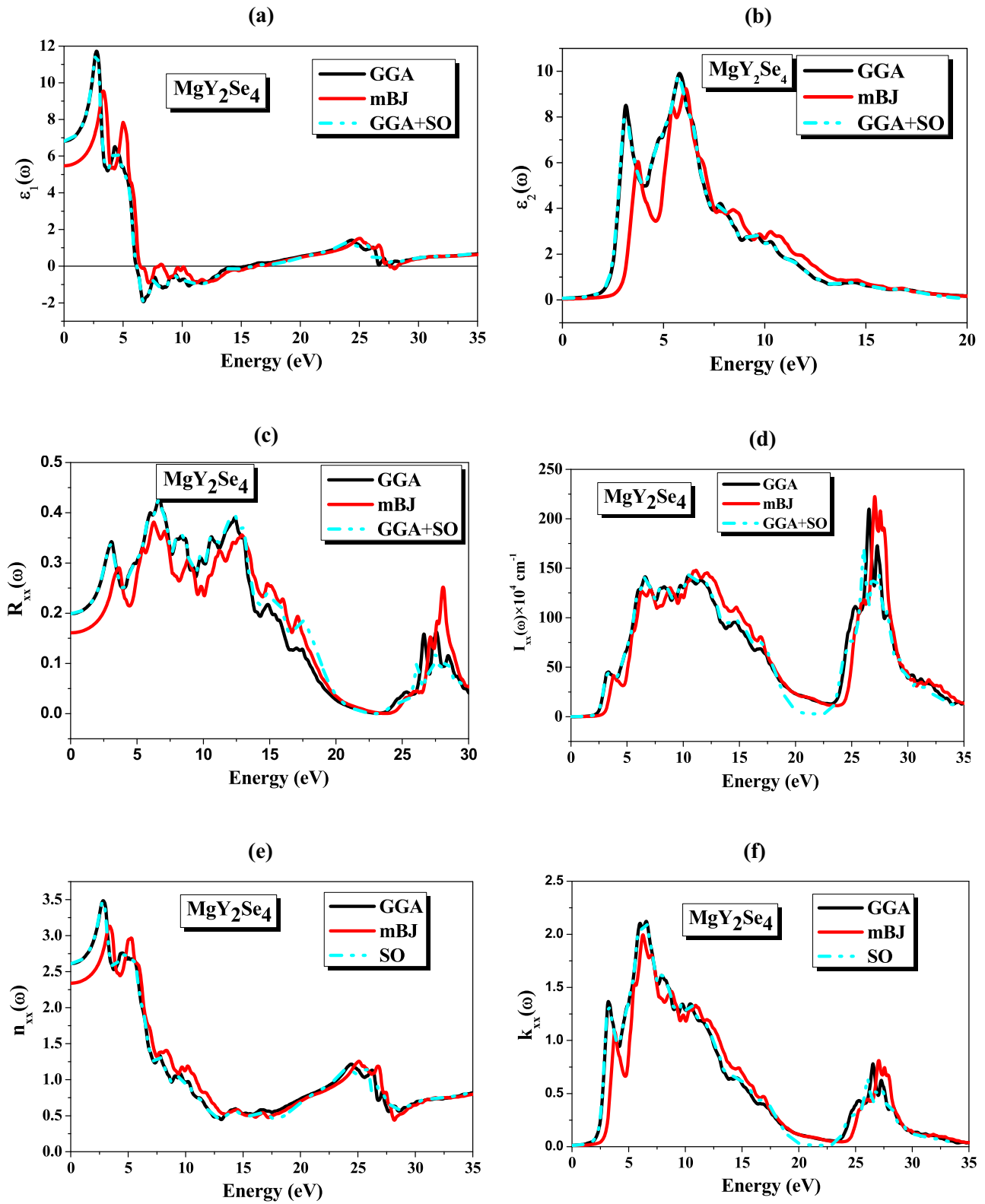
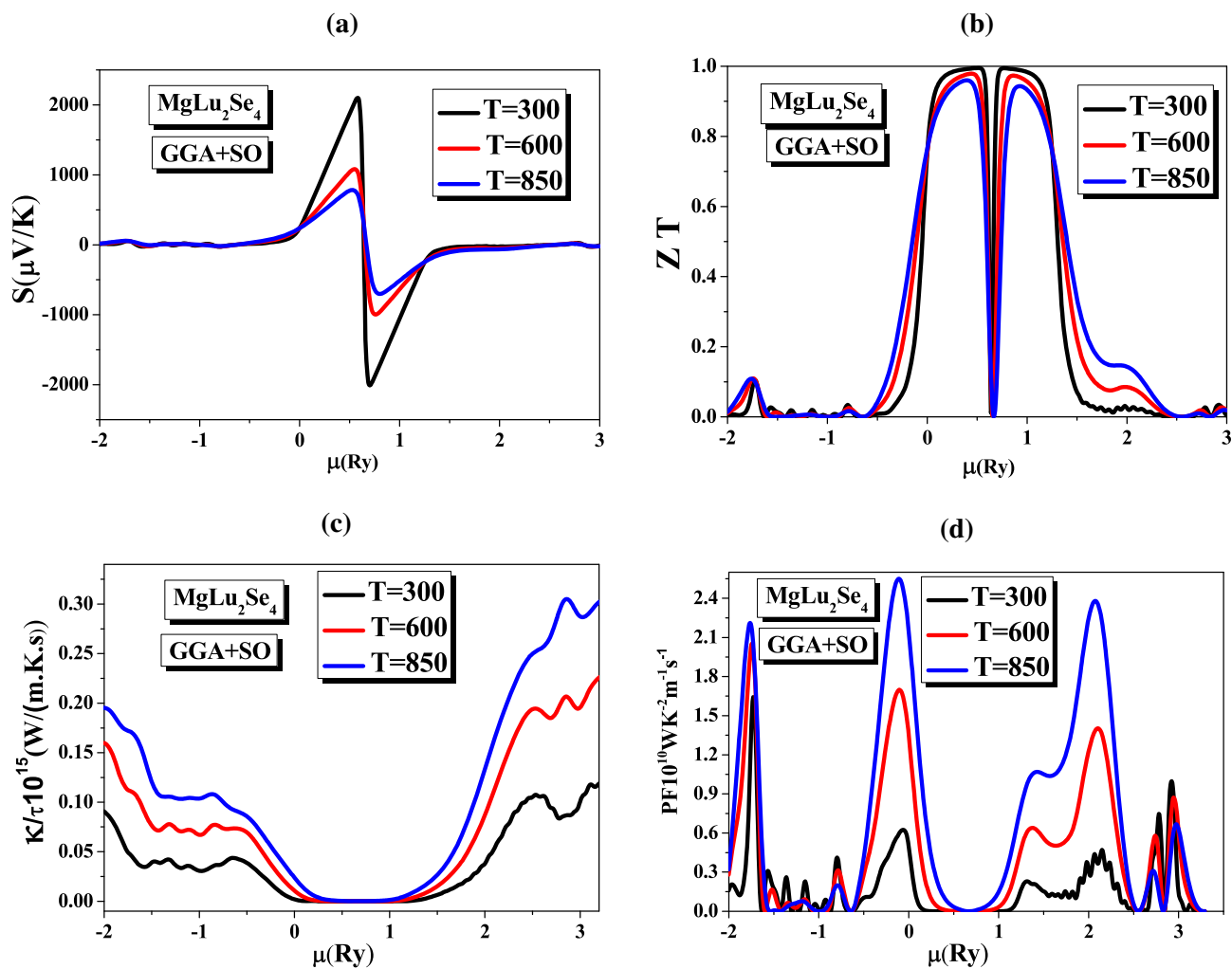


Figure 8. Spectra of (a) real and (b) imaginary dielectric functions, (c) refractive index, (d) extinction coefficient, (e) absorption coefficient and (f) reflectivity of MgY_2Se_4 calculated by GGA, mBJ–GGA and GGA+SO.

Table 5. Static dielectric constant and refractive index of MgX_2Se_4 ($X = \text{Lu}, \text{Y}$) spinels using GGA, mBJ-GGA and GGA+SO approximations.

Approach	$\epsilon_1(0)$			$n(0)$		
	GGA	GGA-mBJ	GGA+SO	GGA	GGA-mBJ	GGA+SO
MgLu_2Se_4	6.88	5.25	6.89	2.62	2.29	262
MgY_2Se_4	6.81	5.47	6.81	2.61	2.33	2.60

**Figure 9.** (a) Seebeck coefficient, (b) figure of merit, (c) thermal conductivity and (d) power factor for MgLu_2Se_4 calculated by GGA+SO computed using BoltzTrap code.

(2.153–2.44 eV) for MgLu_2Se_4 (MgY_2Se_4) and stimulates the transition of electrons. The absorption in the two spinels is maximum ($\approx 140.10^4 \text{ cm}^{-1}$) in the ultraviolet range (5–15 eV), which can be used in molecular absorption spectrophotometry or molecular fluorescence. Optical characteristics, such as absorption and thermal conductivity are influenced by the interaction of electrons with photons. The rate of absorption or transmission of

light influences in the generation of electron–hole pairs. The ultraviolet absorption values and the band gap are factors that favour these two spinels as absorbers in solar cells. In the visible region located between 1.5 and 3.5 eV, MgLu_2Se_4 reflects 15–25% of the incident radiation, while MgY_2Se_4 reflects 17–28%. The reflectivity is lower for mBJ-GGA functional compared with two other approximations. It is pointed out that the peaks of all the

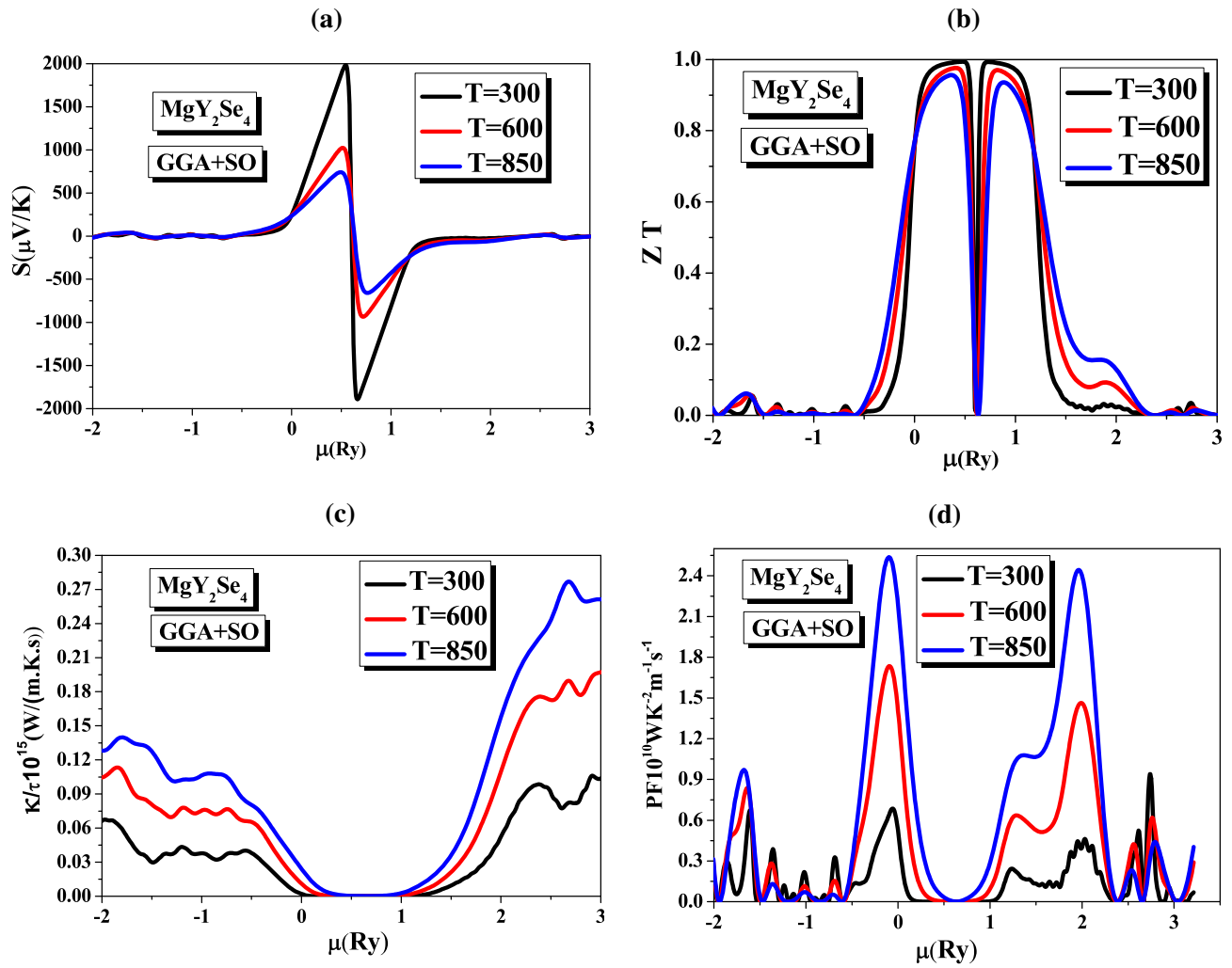


Figure 10. (a) Seebeck coefficient, (b) figure of merit, (c) thermal conductivity and (d) power factor for MgY_2Se_4 calculated by GGA+SO computed using BoltzTrap code.

optical quantities studied relating to the mBJ–GGA functional are shifted to the right compared with GGA and GGA+SO approximations.

3.4 Thermoelectric characteristics

Band structure and electronic transitions play an important role in optical and thermoelectric properties. Phonons contribute to both thermal transports. We study the phenomenon of transport as a function of chemical energy at 300, 600 and 850 K within GGA+SO and BoltzTrap code, through Seebeck coefficient, figure of merit (ZT), thermal conductivity and power factor. The chemical potential is positive for n-type material and negative for p-type material. Seebeck coefficient is the sensitivity of the induced voltage to the temperature gradient across a material. The effect of temperature and chemical potential on Seebeck

coefficient of MgLu_2Se_4 and MgY_2Se_4 is displayed in figures 9a and 10a. Energy levels and band gaps influence the rate of conversion of temperature differences into the voltage. The temperature gradient generates an induced thermoelectric current, which aids in heat transfer according to Thomas Seebeck. The maximum Seebeck value of 2100.12 and 1983.7 $\mu\text{V K}^{-1}$ is obtained at room temperature in p-type region for MgLu_2Se_4 and MgY_2Se_4 . It can be seen that the Seebeck value decreases with increasing temperature, and its value at the Fermi level ($\mu = 0$) is 253.06 and 247.07 $\mu\text{V K}^{-1}$ for MgLu_2Se_4 and MgY_2Se_4 . These positive values explain that these two spinels are p-type semiconductors. The Seebeck coefficient is slightly symmetric with respect to origin point because of the mass difference between electrons and holes. The dependence of ZT on temperature and chemical potential for MgLu_2Se_4 and MgY_2Se_4 is reported in figures 9b and 10b. ZT is a dimensionless quantity that provides information on

thermoelectric efficiency. ZT in p- and n-type regions for MgLu_2Se_4 and MgY_2Se_4 are nearly identical. It is reported that the ZT for p- and n-type regions are symmetrical with respect to Fermi level axis. ZT is close to unity with optimum value at ambient temperature on both sides in the vicinity of Fermi level. The crystal structure of a material affects its thermal conductivity and optical transparency. A material with a thermoelectric potential shows low thermal conductivity. The maximum of thermal conductivity in the p- and n-type regions is 0.2 and $0.3 \text{ W m}^{-1} \text{ K}^{-1} \text{ s}^{-1}$ (0.13 and $0.27 \text{ W m}^{-1} \text{ K}^{-1} \text{ s}^{-1}$) for MgLu_2Se_4 and MgY_2Se_4 . From this result, we deduced that MgY_2Se_4 is more performing as thermoelectric material than MgLu_2Se_4 . A thermoelectric material converts waste heat into electrical energy. The transport of these charge carriers is decisive in thermoelectric performance. High optical absorption of a material implies that incident light is absorbed and converted to heat. The thermal conductivity is caused by free electrons. The effect of temperature on thermal conductivity is displayed in figures 9c and 10c. We note that for n- and p-type regions, the peak magnitude of thermal conductivity increases when the temperature is enhanced. Compound with strong covalent bonds have lower thermal conductivity and those with good optical transparency often have weaker bonds with significant electron and phonon scatterings. We also note the presence of a valley located on either side of the Fermi level, where the thermal conductivity is low and has the same width in the two spinels, which can be explained by their neighbouring band gap. The maximum observed conductivity is $0.28 \times 10^{15} \text{ W m}^{-1} \text{ K}^{-1} \text{ s}^{-1}$ located in the n-type region and corresponds to a chemical potential of about 2.75 Ry at 850 K . The conductivity increases almost continuously in the p-type region, while in the n-type region, the growth is followed by some oscillations. Power factor is the product of the square of the Seebeck coefficient with the electrical conductivity ($\text{PF} = S^2\sigma$), so, it is positive. The effect of temperature and chemical potential on power factor is visualized in figures 9d and 10d. The power factor is a parameter that determines the strength of a material. The maximum of PF in the p-type region is greater than that which corresponds to the n-type region. The spinel having a large Seebeck value exhibits a greater power factor value. A thermoelectric material shows lattice stability, low thermal conductivity and high ZT. The study of the thermoelectric characteristics shows that these two spinels are candidates in thermoelectric application, but MgY_2Se_4 is more advantageous.

4. Conclusions

Ab initio electronic structure calculations indicate that MgLu_2Se_4 (MgY_2Se_4) is direct Γ - Γ band gap semiconductor of 1.4 , 2.44 and 1.253 eV (1.312 , 2.153 and 1.178 eV) using GGA,

mBJ-GGA and GGA+SO functionals. The high absorption in the ultraviolet range for the two spinels, their adequate band gap and refractive index factors favour them as absorbers in solar cells. The lattice stability and maximum power factor in the p-type region, zenith value close to unity at ambient temperature, large Seebeck coefficient, lower thermal conductivity and high ZT make these two spinels as candidates in thermoelectric application. The main effect of replacing Lu ions by Y ions is a reduction in the band gap by about 0.08 , 0.28 and 0.07 eV . Origins of the electronic conductivity observed can be related to the existence of intrinsic defects Mg, Y, Lu and Se vacancies and the presence of undesired electron conducting secondary phases in the MgLu_2Se_4 and MgLu_2Se_4 . The lack of the experimental results for MgX_2Se_4 ($X = \text{Lu}, \text{Y}$) could be useful for other investigations. The two spinels under study are chemically and elastically stable. The PDOS in valence band shows the hybridization between Se-p and X-d sites for MgX_2Se_4 ($X = \text{Lu}, \text{Y}$), which reflects their covalent bonding.

Acknowledgement

This work was funded by the Researchers Supporting Project No. RSPD2024R551, King Saud University, Riyadh, Saudi Arabia.

References

- [1] Wang P, Zhao-Karger Z, Klein F, Chable J, Braun T, Schür A R *et al* 2019 *ChemSusChem* **12** 2286
- [2] Bouferrache K, Ghebouli M A, Slimani Y, Ghebouli B, Fatmi M, Alomairy S *et al* 2018 *Energy Environ. Sci.* **11** 1945
- [3] Bouferrache K, Ghebouli M A, Ghebouli B, Fatmi M, Chihi T, Algethami N *et al* 2023 *Solid State Commun.* **377** 115366
- [4] Wang Y, Chen W, Liu F, Yang D, Tian Y, Ma C *et al* 2019 *Physics* **13** 102180
- [5] Bitla Y, Chin Y-Y, Lin J-C, Van C N, Liu R, Zhu Y *et al* 2015 *Sci. Rep.* **5** 15201
- [6] Wittingham M S 2004 *Chem. Rev.* **104** 4271
- [7] Wittingham M S 2014 *Chem. Rev.* **114** 11414
- [8] Shanmugavani A and Selvan R K 2016 *Electrochim. Acta* **188** 852
- [9] Zareef F, Rashid M, Ahmadini AAH, Alshahrani T, Kattan NA, Laref A 2021 *Mater. Sci. Semicond. Process.* **127** 105695
- [10] Mustafa G M, Noor N A, Waqas M, Sajjad M, Naeem M A, Mahmood Q *et al* 2021 *Mater. Sci. Semicond. Process.* **121** 105452
- [11] Pham K D, Batouche M, Si Mohammed D E, Seddik T, Tuan V, Dat D *et al* 2021 *J. Solid State Chem.* **293** 121763
- [12] Schwarz K, Blaha P and Madsen G K H 2002 *Comput. Phys. Commun.* **147** 71

- [13] Perdew J P, Burke K and Ernzerhof M 1996 *Phys. Rev. Lett.* **77** 3865
- [14] Becke A D and Johnson E R 2006 *J. Chem. Phys.* **124** 221101
- [15] Anisimov V I and Gunnarsson O 1991 *Phys. Rev. B* **43** 7570
- [16] Blaha P, Schwarz K, Sorantin P I and Trickey S B 1990 *Comput. Phys. Commun.* **59** 399
- [17] Brik M G, Suchocki A and Kaminska A 2014 *Inorg. Chem.* **53** 5088
- [18] Al-Qaisi S, Rai D P, Alshahrani T, Ahmed R, Haq B U, Tahir S A *et al* 2021 *Mater. Sci. Semicond. Process.* **128** 105766
- [19] Huntington H B 1958 *Solid State Phys.* **7** 213

Springer Nature or its licensor (e.g. a society or other partner) holds exclusive rights to this article under a publishing agreement with the author(s) or other rightsholder(s); author self-archiving of the accepted manuscript version of this article is solely governed by the terms of such publishing agreement and applicable law.